Biomaterials 139 (2017) 202–212

Contents lists available at ScienceDirect

Biomaterials

journal homepage: www.elsevier.com/locate/biomaterials

Tissue-engineered hypertrophic chondrocyte grafts enhanced long bone repair

Jonathan Bernhard [a], James Ferguson [b], Bernhard Rieder [c], Patrick Heimel [b, d], Thomas Nau [b], Stefan Tangl [d], Heinz Redl [b], Gordana Vunjak-Novakovic [a, e, *]

[a] Department of Biomedical Engineering, Columbia University, New York, NY 10032, USA
[b] Ludwig Boltzmann Institute of Experimental and Clinical Traumatology, Austrian Cluster for Tissue Regeneration, Vienna A-1200, Austria
[c] Department of Biochemical Engineering, University of Applied Sciences Technikum Wien, Austrian Cluster for Tissue Regeneration, Vienna A-1200, Austria
[d] Department of Oral Surgery, Medical University Vienna, Austrian Cluster for Tissue Regeneration, Vienna A-1090, Austria
[e] Department of Medicine, Columbia University, New York, NY 10032, USA

ARTICLE INFO

Article history:
Received 10 April 2017
Received in revised form
25 May 2017
Accepted 27 May 2017
Available online 31 May 2017

Keywords:
Bone regeneration
Bone tissue engineering
Hypertrophic chondrocytes
Endochondral ossification

ABSTRACT

Bone has innate ability to regenerate following injury. However, large and complex fractures exceed bone's natural repair capacity and result in non-unions, requiring external intervention to facilitate regeneration. One potential treatment solution, tissue-engineered bone grafts, has been dominated by recapitulating intramembranous ossification (bone formation by osteoblasts), although most serious bone injuries heal by endochondral ossification (bone formation by remodeling of hypertrophic cartilaginous anlage). The field has demonstrated that using endochondral ossification-based strategies can lead to bone deposition. However, stem cell differentiated hypertrophic chondrocytes, the key cell type in endochondral ossification, have not been studied for long bone defect repair. With translation in mind, we created tissue-engineered grafts using human adipose stem cells (ASC), a clinically relevant stem cell source, differentiated into hypertrophic chondrocytes in decellularized bone scaffolds, and implanted these grafts into critical-size femoral defects in athymic rats. Over 12 weeks of implantation, these grafts were compared to acellular scaffolds and grafts engineered using ASC-derived osteoblasts. Grafts engineered using hypertrophic chnodrocytes recapitulated endochondral ossification, as evidenced by the expression of genes and proteins associated with bone formation. Markedly enhanced bone deposition was associated with extensive bone remodeling and the formation of bone marrow, and with the presence of pro-regenerative M2 macrophages within the hypertrophic grafts. As a result, hypertrophic chondrocyte grafts bridged 7/8 defects, as compared to only 1/8 for osteoblast grafts and 3/8 acellular scaffolds. These data suggest that ASC-derived hypertrophic chondrocytes in osteogenic scaffolds can improve long bone repair.

1. Introduction

An estimated 100,000 bone fractures per year exceed the regenerative ability of native bone and remain unhealed, with the clinical presentation of fracture non-unions [1]. To effectively treat non-unions, an external intervention is required. In situations requiring grafting material, autografts promote faster union formation and decrease the rate of surgical revisions compared to allografts [2]. Despite positive clinical outcomes, the use of autografts remains limited due to the scarcity of suitable autologous bone and the associated donor site morbidity [3]. As a possible treatment option, autologous bone grafts can be engineered *in vitro* from the patient's stem cells, to offer bone grafting without the necessity of harvesting bone from the patient [4,5]. By combining osteogenic cells, osteoinductive scaffolds, and external stimuli, experimental bone grafts resembling autologous grafts have been engineered [6]. However, the use of these grafts to repair long bone non-unions have produced mixed results [6,7].

In the case of long bone repair, the body utilizes endochondral ossification [8,9]. During endochondral ossification, the initial fracture is stabilized by the formation of a cartilage anlage by mesenchymal stem cells [10,11]. As the initial anlage-building

* Corresponding author. 622 West 168th Street, Vanderbilt Clinic Room 12-234, New York, NY 10032, USA.
E-mail address: gv2131@columbia.edu (G. Vunjak-Novakovic).

http://dx.doi.org/10.1016/j.biomaterials.2017.05.045
0142-9612/

chondrocytes mature into hypertrophic chondrocytes, they start controlling the turnover of the cartilage anlage into a bone template, and induce formation of vasculature and bone marrow [9–11]. Previous work has shown that initiating endochondral ossification [12–16] or including hypertrophic chondrocytes [17–21] *in vivo* will lead to bone formation. Due to the superior outcomes of autologous grafts [2] and the limitations associated with cell and factor therapies [7], we aimed to engineer clinically relevant, controllable, and reproducible tissue grafts for long bone repair. Based on these previous studies, we utilized differentiated hypertrophic chondrocytes within a suitable tissue engineered construct to facilitate bone formation and defect healing by mobilizing native-like processes.

To provide the stable environment necessary for effective long bone repair [22], and provide mechanical properties of the native skeleton, decellularized bone scaffolds were utilized. Adipose derived stem cells (ASCs) were used, because they are multipotent with similar capability as bone marrow stromal cells, Fig. S2 [23], easy to harvest, can be expanded to clinically relevant numbers to allow creation of autologous tissues [24], and were recently shown to have hypertrophic chondrocyte differentiation capability [25]. The protocols utilized for tissue engineering were based on previous studies that utilized embryonic [26] and bone marrow stem cells [18,27]. With the creation of these unique hypertrophic chondrocyte bone tissue grafts, we studied their ability to repair orthotopic, critical-size defects in the rat femur, in a model of long bone fracture healing. To compare the performance of these constructs to the established tissue engineered grafts, we created complementary, osteoblast-based bone grafts optimized in a perfusion-controlled bioreactor [28,29], and used acellular scaffolds as an additional control. Based on the previous studies highlighted above, and the natural path of bone repair, we hypothesized that the differentiation of hypertrophic chondrocytes would result in more effective bone repair than traditional tissue engineered approaches. We found that the differentiated hypertrophic chondrocytes created robust, hypertrophic cartilage templates within the decellularized bone scaffolds. Upon implantation, the grafts mediated fast remodeling and integrated with the native bone to bridge critical size femoral defects, in contrast to either of the two groups that produced smaller amounts of new bone, and in most cases failed to bridge the defects. The results suggest the feasibility of hypertrophic chondrocyte-based tissue engineered grafts for long bone repair.

2. Materials and methods

All materials were obtained from Sigma-Aldrich (St. Louis, MO, USA) unless otherwise noted.

2.1. Scaffold preparation

Trabecular bone was harvested from bovine juvenile wrists as in our previous studies [29], and cut into cylinders 4 mm diameter by 6 mm high. The initial material was sorted by bulk density (mass/volume) to provide consistent porosity and void volume among the scaffolds, and the bulk densities in the range 0.35–0.50 g/mL were used as in our previous studies [30]. Scaffolds were decellularized following published protocols [29]. Briefly, scaffolds were washed in a series of solutions: 1) 0.1% EDTA in PBS for 1 h, 2) hypotonic buffer consisting of 10 mM Tris and 0.1%EDTA in PBS for 12 h at 4 degrees Celsius, 3) detergent consisting of 10 mM Tris and 0.5% SDS in PBS for 24 h at room temperature on an orbital shaker at 300 revolutions per minute, 4) enzymatic solution of 100 units/mL DNase and 1 unit/mL of RNase with 10 mM Tris in PBS at 37 degrees Celsius for 6 h. After multiple washes in PBS, scaffolds were frozen and lyophilized.

2.2. Cell isolation, expansion, and seeding into decellularized bone scaffolds

Adipose tissue was obtained with informed consent from the patient and the ethical board of Upper Austria at the Rotes Kreuz facility in Linz, Austria, and adipose stem cells were isolated as previously described [24,31]. The ability of the cells to give rise to chondrocytes, osteoblasts and adipocytes was verified by tri-differentiation testing and were positive for CD73, CD90, CD105, and negative for CD34 and CD14 by fluorescence-activated cell sorting (FACS) analysis (Fig. S1). The donor (Adipose Donor 1 in Fig. S2) was selected from three potential donors based on cell expansion numbers. Cells were expanded until passage 4 in expansion medium consisting of high glucose medium with L-glutamine, 10% fetal bovine serum, 1% penicillin/streptomycin, and 1 ng/mL basic fibroblast growth factor. In preparation for seeding, decellularized bone (DCB) scaffolds were incubated in 70% ethanol for 2 days and then in sterile culture medium for 1 day. P4 adipose derived stem cells were trypsinized, resuspended in culture medium, and infused into dried DCB scaffolds at a volume density of 30 million cells/mL of DCB scaffold volume. As the prepared scaffolds had an estimated volume of 75 μL, 2.25 M cells were seeded.

2.3. Bone tissue engineering

Cell-seeded scaffolds were incubated in expansion medium for 2 days, to allow cell attachment, and divided into an experimental graft group, hypertrophic chondrocytes in static culture, and an engineered graft control, with osteoblasts in perfusion culture. The *hypertrophic chondrocyte* grafts, denoted here as *H* group, were formed by a two-step culture schematic, all under static conditions, using previously established methods [18,27]. Grafts were first cultured for 2 weeks in chondrogenic medium (high glucose DMEM, ThermoFisher, Waltham, MA; 100 nM dexamethasone; 50 μg/mL ascorbic acid; 50 μg/mL proline; 100 μg/mL sodium pyruvate; 1% ITS+; 1% P/S; 10 ng/mL BMP6; 10 ng/mL TGF-β3). For the subsequent 3 weeks, the medium was changed to hypertrophic medium (high glucose DMEM, ThermoFisher, Waltham, MA; 1 nM dexamethasone; 50 μg/mL ascorbic acid; 50 μg/mL proline; 100 μg/mL sodium pyruvate; 1% ITS+; 1% P/S; 50 ng/mL of L-thyroxine; 5 mM of β-glycerophosphate).

The *osteoblast* grafts, denoted here as *O* group, were formed in osteogenic culture medium using a bioreactor system with perfusion. The perfusion rate was set to correspond to the interstitial flow velocity of 400 μm/s that was established in our previous study [28] as optimal for osteoblast differentiation. The bioreactor system and the methods used to culture osteoblast-based tissue engineered bone were identical to those that established the strong osteoblast differentiation and bone deposition of ASCs in our previous studies [32]. The cultivation was for 5 weeks, in osteogenic medium (low glucose DMEM, ThermoFisher, Waltham, MA; 100 nM dexamethasone; 50 μg/mL ascorbic acid; 10 mM HEPES buffer; 10% fetal bovine serum; 1% P/S; 5 mM β-glycerophosphate), culture medium was changed twice a week. At the end of 5 weeks of cultivation, tissue engineered grafts were evaluated and implanted into orthotopic defects created in the right femur of a nude rat.

The *control* grafts, denoted here as the *Con* group, were the acellular DCB scaffold sterilized in 70% ethanol for 2 days and then left in sterile phosphate buffered saline until surgery.

2.4. Critical-sized defect creation and graft implantation

Animal studies were conducted under an approved protocol and

with the permit of the municipal government of Vienna, Austria. The experiments were consistent with the Guide for the Care and Use of Laboratory Animals of the National Institute of Health (revised 2011). Twenty-eight male, RNU nude rats were used. Animals were kept in housing cages with filter tops, in groups of two, and separate from other animals. At the time of surgery, the rats weighed between 260 and 392 g. Preoperatively, the animals were administered subcutaneously 0.05 mg/kg buprenorphine (Bupaq, Richterpharma AG, Austria) and 4 mg/kg carprofen (Rimadyl, Zoetis Osterreich Gesm.b.H, Austria). Anesthesia was induced with isoflurane (Forane, AbbVie Gesm.b.H, Austria) and maintained with 1.5–2.5% isoflurane/oxygen by way of mask inhalation.

Once the animal was under stable anesthesia, a lateral approach was used to expose the right femur. After fixation with a four-pin, POM fixator (modified from the method described in Ref. [33]), a defect of 5 mm was created with a Gigli wire saw. Grafts were placed into the defect and the muscle and skin were sutured around the graft and the fixator, respectively. For each experimental group (H, O, Con), eight rats underwent implantation, with four rats not receiving implants to confirm the non-healing in critical-size defects. 0.05 mg/kg buprenorphine and 4 mg/kg carprofen were given subcutaneously over the first four days post-implantation to manage pain, and discontinued thereafter. The rats with an open defect and no implant experienced fixator failure between 6 and 9 weeks, and were euthanized, demonstrating a defect that had a non-healing non-union. Twelve weeks post-implantation, the rats were euthanized by an overdose injection of intracardially delivered thiopental sodium while under deep isoflurane anesthesia. The right femur of each animal was harvested for detailed characterization.

2.5. Micro-computed tomography (μCT) and defect bridging determination

Animals were scanned at a 50 μm resolution by μCT at day 1, and at 3, 6, and 9 weeks post-implantation, using a vivaCT 75 (Scanco Medical, Bruttisellen, Switzerland) preclinical scanner. Rats were anesthetized with 2% isoflurane throughout the duration of the scan. The right femur was scanned at an isotropic resolution of 50 μm. Scans were reconstructed to provide 3D representations of the defect area. After femur harvest at 12 weeks, μCT scans were performed on a μCT 50 (Scanco Medical, Bruttisellen, Switzerland) at an isotropic resolution of 10 μm. Scans were reconstructed to provide 3D representations of the defect, and quantitative data for the bone volume and bone surface to volume ratio within the defect was calculated using the Scanco Medical morphometry software. Bridging was defined as the formation of a continuous segment of mineralized bone along a vertical plane that spanned the defect, and visualized through the μCT image slices and 3D reconstruction. Two blinded researchers went through the slices and 3D reconstruction, and independently determined bridging. If both researchers agreed on bridging, the sample was considered bridged and given a 1, if the researchers disagreed on bridging, the sample was considered incomplete bridging, and given a 0.5.

2.6. Quantitative biochemical analysis

For pre-implantation analysis, grafts were cut in half and the wet weights were recorded. Graft halves were digested with papain (40 Units/mg) in digest buffer (0.1 M sodium acetate, 10 mM cysteine HCl and 50 mM EDTA, pH 6.0) at 60 °C overnight. DNA content was measured from the digest using Quant-iT PicoGreen assay kit and the supplied lambda DNA standard (ThermoFisher, Waltham, MA). Sulfated glycosaminoglycan (GAG) content was measured using the dimethylmethylene blue dye assay with chondroitin 6 sulfate as a control. Calcium quantitation was not performed due to the calcified nature of the decellularized scaffolds, and the confounding factor that played in the analysis. For each assay, n = 4 biological replicates were used per group and time point.

2.7. Real time RT-PCR

Pre-implantation, total RNA was extracted using the Trizol method (ThermoFisher, Waltham, MA). DNase I treatment was utilized for 10 min at 37 °C to remove any contaminating DNA. cDNA was transcribed using the High Capacity cDNA Reverse Transcription kit (ThermoFisher, Waltham, MA) according to the manufacturer's instructions. Quantitative RT-PCR was performed using Fast Sybr Green mix (ThermoFisher, Waltham, MA). Expression levels were quantified applying the ΔC_t method, with the C_t of GAPDH subtracted from the C_t of the gene of interest. Forward and reverse primers for each gene are presented in Table 1. Samples were evaluated using n = 5 biological replicates per experimental group and time point.

2.8. Pre-implantation histology and immunohistochemistry

Grafts were fixed in 10% formalin, rinsed in PBS, and decalcified using a formic acid based solution (Immunocal Decalcifier, StatLab, McKinney, TX). After decalcification, grafts were washed multiple times with PBS, dehydrated, embedded in paraffin, and sectioned at 6 μm. Histological sections were stained with alcian blue for GAG (Pre-Implantation) following standard protocols, and Movat's Pentachrome (Pre- and Implantation) following manufacturer's instructions. Antigen retrieval was conducted prior to immunohistochemistry. Slides were placed into a container filled with citrate buffer (1.8 mM citric acid, 8.2 mM sodium citrate, pH 6.0), and the container was submerged in boiling water for 20 min. Slides were blocked with 0.3% hydrogen peroxide in absolute methanol for 30 min before using the Vectastain Elite Universal staining kit (Vector Laboratories, Burlingame, CA). The primary antibodies for BSP (Pre-Implantation, EMD Millipore, 1/500 dilution, AB1854, Bilerica, MA), and OPN (Pre-Implantation, Abcam, 1/200 dilution, AB166709, San Francisco, CA) were incubated overnight at 4 °C. The slides were counterstained with Hematoxylin QS (Vector Laboratories, Burlingame, CA). Staining for collagen type X was conducted as previously described [34]. The primary antibody was obtained from Abcam (Pre-Implantation, 1/1000 dilution, AB49945, San Francisco, CA); Hematoxylin QS was used as a counterstain.

2.9. Hard bone histology

Femurs with the attached fixation devices were immersed in 4%

Table 1
Primers used in RT-PCR.

Gene	Forward	Reverse
RUNX2	CCGTCTTCACAAATCCTCCCC	CCCGAGGTCCATCTACTGTAAC
COL1A1	GATCTGCGTCTGCGACAAC	GGCAGTTCTTGGTCTCGTCA
MMP13	CCAGACTTCACGATGGCATTG	GGCATCTCCTCCATAATTTGGC
ALPL	GGGACTGGTACTCAGACAACG	GTAGGCGATGTCCTTACAGCC
IBSP	GAACCTCGTGGGGACAATTAC	CATCATAGCCATCGTAGCCTTG
COL10A1	CATAAAAGGCCCACTACCCAAC	ACCTTGCTCTCCTCTTACTGC
SOX9	AGCGAACGCACATCAAGAC	CTGTAGGCGATCTGTTGGGG
COL2A1	AGACTTGCGTCTACCCCAATC	GCAGGCGTAGGAAGGTCATC

neutral-buffered formaldehyde solution, then dehydrated in ascending grades of ethanol and imbedded in light curing resin (Technovit 7200 VLC; Kulzer & Co., Wehrheim, Germany). Thin ground sections along the longitudinal axis of the shaft oriented in a frontal plane were cut using a previously developed method [35] and stained with Levai-Laczko dye [36]. Histological specimens were digitized with the Olympus dotSlide 2.4, digital virtual microscopy system (Olympus, Japan, Tokyo) at a resolution of 0.32 μm. Semi-quantitative values for the amount of new bone deposited, the area of old bone, the area of fibrous tissue, the area of bone marrow, and the quantity and location of osteoclasts were determined in a blinded fashion on the stained samples within the defect area by two independent researchers using n = 4 femurs per staining. Levai-Laczko staining is a common stain used in calcified tissues that demonstrates the presence of several components related to bone and cartilage. Through the multiple staining components, it allows the identification of bone of different maturities, cartilage, calcified cartilage, bone marrow, and general fibrous tissue.

2.10. Post-implantation histology and immunohistochemistry

The femurs for immunostaining were submerged in 4% neutral-buffered formaldehyde solution for 24 h, followed by extensive washing in PBS. Femurs were decalcified using Immunocal (StatLab, McKinney, TX), followed by extensive washing in PBS and graded ethanol dehydration. Sections of the femur were made 6 μm thick, and histology was stained with Movat's Pentachrome following manufacturer's instructions. Immunohistochemistry was performed following the published citrate buffer antigen retrieval methods. Vectastain rabbit antibody kit (PK-4001, Vector Laboratories, Burlingame, CA), and AbCam's mouse on mouse kit (AB127055, San Francisco, CA) were utilized to stain for CD163 (Abcam, 1/500, AB182422). Semi-quantitation of the stainings was conducted in ImageJ, by first isolating the defect area, converting the images to 8-bit greyscale profile, and then indicating a threshold that allowed the isolation of positively-stained CD163 + cells, and finally using the ImageJ automatic particle analyzer with settings at 0.1–1.0 circularity and 10–200 microns^2 size. This process was completed on n = 3 biological replicates per group.

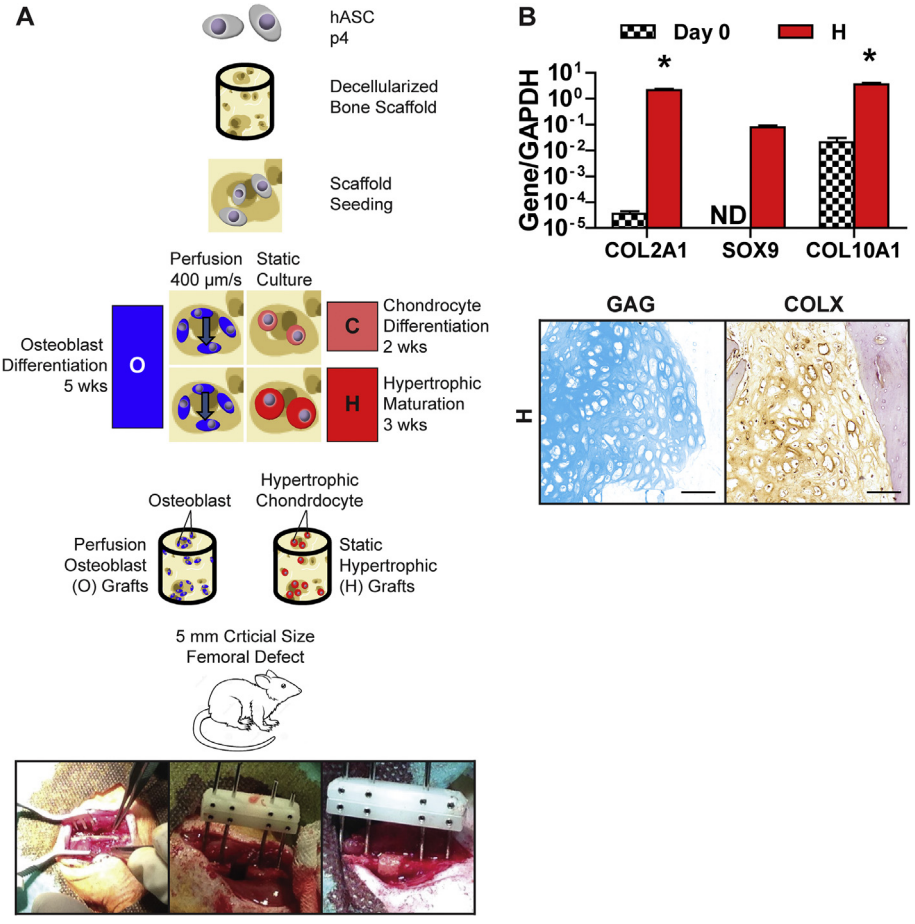

Fig. 1. A Experimental methodology and the creation of tissue engineered grafts. Tissue engineered grafts were constructed by seeding human adipose derived stem cells (ASCs), a clinically relevant source of mesenchymal stem cells, into decellularized bone scaffolds. *Hypertrophic chondrocyte grafts* (H) were cultured statically by differentiating ASCs for 2 weeks in chondrogenic medium, and maturing the cells to hypertrophic chondrocytes for 3 weeks in hypertrophic medium. *Osteoblast grafts* (O) were generated from ASCs under perfusion of osteogenic medium for 5 weeks in bioreactors. Both groups of tissue engineered grafts, along with an acellular scaffold control, were implanted into an orthotopic, 5 mm critical-size defect created in the femur of athymic rats. The femur, but not the graft, was stabilized with an internal fixator. Bone deposition was monitored through micro computed tomography (μCT) at the time of implantation, and at 3, 6, and 9 weeks post-implantation. At the 12-week endpoint, femurs were harvested, and regeneration of the defect was evaluated in detail. **B Verification of hypertrophic chondrocyte differentiation within tissue engineered grafts.** Gene expression of key chondrogenic and hypertrophic genes were significantly increased, demonstrating chondrocyte differentiation and hypertrophic maturation of the resulting chondrocytes. Histological sections of cultured H grafts demonstrated glycosaminoglycan (GAG) deposition, indicating chondrocyte differentiation. Immunohistochemistry demonstrated collagen type X deposition, strongly present surrounding the enlarged lacunae of the hypertrophic chondrocytes, indicating hypertrophic maturation. Value ± SD. Significant differences between the groups: $^*p < 0.05$ (n = 3); Scale bars: 100 μm.

2.11. Statistics

Statistically significant differences between the two experimental groups during pre-implantation testing were evaluated using a Student's T-Test, $\alpha = 0.05$, with significance determined by $p < 0.05$ (Prism Software, GraphPad, La Jolla, CA, USA). Statistical significance of differences between the groups and time points was determined by using a one-way analysis of variance (ANOVA) followed by Tukey's post-test, $\alpha = 0.05$, with significance determined by $p < 0.05$.

3. Results

3.1. Bone formation in vitro by hypertrophic chondrocytes (endochondral ossification) and osteoblasts (intramembranous ossification)

Differentiation of ASCs into hypertrophic chondrocytes and osteoblasts was induced for cells cultured in decellularized bone (DCB) scaffolds, by adding appropriate molecular factors to culture medium, under either static conditions (hypertrophic chondrocytes) or interstitial flow (osteoblasts) (Fig. 1). Static hypertrophic chondrocyte grafts (H group) were differentiated by inducing chondrogenesis and cartilage tissue formation for 2 weeks, and then inducing chondrocyte hypertrophy over the subsequent 3 weeks. After 5 weeks of culture, these grafts demonstrated endochondral-like characteristics, with upregulated gene expression of chondrocyte and hypertrophic chondrocyte markers, and deposition of collagen X and glycosaminoglycan around enlarged chondrocyte lacunae (Fig. 1B). Perfused osteoblast grafts (O group) were formed by osteogenic differentiation in a perfusion bioreactor for the entire 5-week culture period. These grafts demonstrated the cellularity and deposition profile of bone matrix similar to those in previous studies (Fig. 2B–D) [28,29].

Expression of bone-related genes was highest in H grafts (Fig. 2A). A master regulator for bone production (RUNX2, expressed in both cell types [11,37–39]), and the genes associated with matrix formation (COL1A1 and MMP13) and mineral deposition (ALPL and IBSP) were all upregulated in the H group. Movat's pentachrome staining (Fig. 2B, red deposition) revealed that H grafts had relatively little osteoid deposition, in stark contrast to the O grafts. Instead, hypertrophic chondrocytes deposited extensive cartilaginous matrix within the scaffold pores (green marks glycosaminoglycan, Fig. 2C). O grafts had high cellularity throughout the graft volume, with widespread and dense deposition of collagenous matrix (collagen fibers are shown in red). Deposition of bone sialoprotein (BSP), a key nucleator for bone mineral formation, correlated with the general matrix characteristics (Fig. 2D). In the H grafts, BSP was located near hypertrophic chondrocytes within the dense cartilage matrix. In the O grafts, BSP was present throughout the graft along the collagen fibers. Osteopontin (OPN), an important protein in bone formation and remodeling, was present throughout the cartilaginous matrix of the H grafts, but was largely absent in the O grafts (Fig. 2E). At the time of implantation, H grafts had superior expression of bone-related genes and extensive deposition of bone forming and remodeling proteins.

3.2. In vivo integration, matrix deposition, and bridging of the defects

H, O and Con grafts were implanted into critical-size 5-mm long defects in the femur of athymic nude rats, a standard orthotopic model for long bone fracture repair (Fig. 1). Live μCT scans, at a resolution of 50 μm, were taken throughout the time of implantation to monitor bone integration and matrix turnover (Fig. 3). At 3 weeks post-implantation, H grafts have already started to integrate into the native bone, and had large mineral depositions along the medial exterior of the graft (Fig. 3B). The O grafts had only minimal integration with the surrounding bone, without apparent mineral deposition. The Con grafts resembled the H grafts with respect to external mineral deposition.

By 6 weeks, the differences in regeneration between the groups became noticeable, as the H grafts had extensive integration along both ends, and a closing bridge along the medial side (Fig. 3C), while the O grafts had only partial integration along both ends. The Con had extensive mineral deposition along the medial side of the

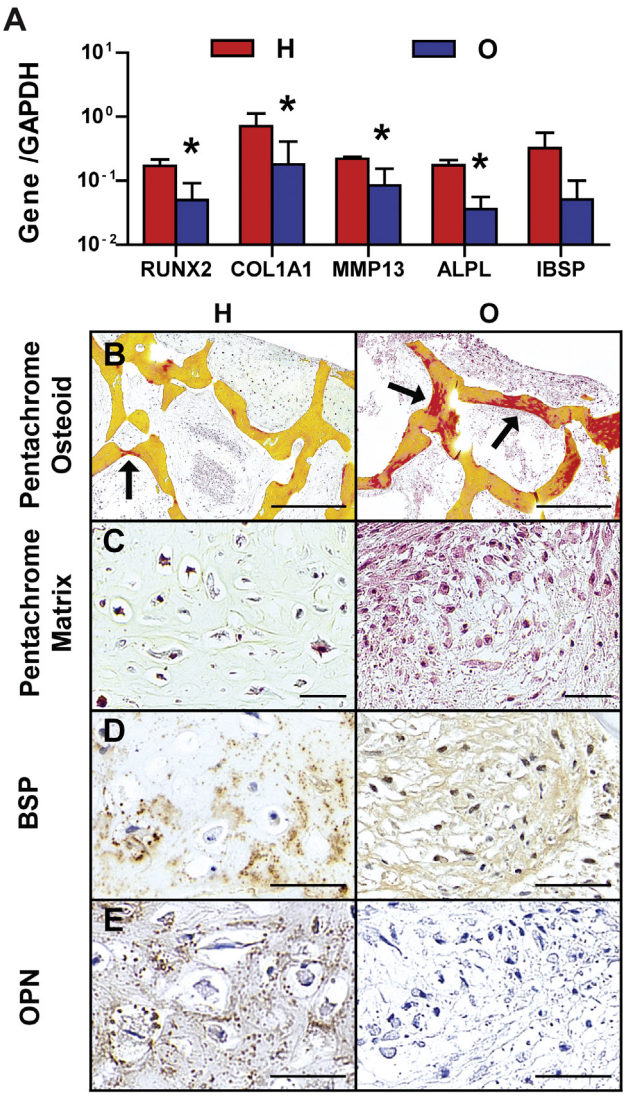

Fig. 2. Composition and behavior of engineered bone grafts *in vitro*. **A** Hypertrophic (H) grafts had significantly enhanced expression of bone development genes when compared to osteoblast (O) grafts. **Histomorphology of hypertrophic (H, left) and osteoblast grafts (O, right)**. **B-C** osteoid and tissue matrix (by pentachrome) demonstrating increased osteoid formation (black arrows, red on yellow scaffold) in the O grafts and a difference in matrix deposition between H grafts (C cartilage, green GAG) and O grafts (F red fibrous tissue) within the DCB bone scaffold (yellow); **E-F** Bone sialoprotein and osteopontin (antibodies) demonstrating the differences in deposition with H grafts depositing around cellular lacunae and O grafts depositing along fibrous tissue. Scale bars: 500 μm (2B), 50 μm (2C, 2D, 2E). Value ± SD. Significant differences between the groups * $p < 0.05$ ($n = 4$). (For interpretation of the references to colour in this figure legend, the reader is referred to the web version of this article.)

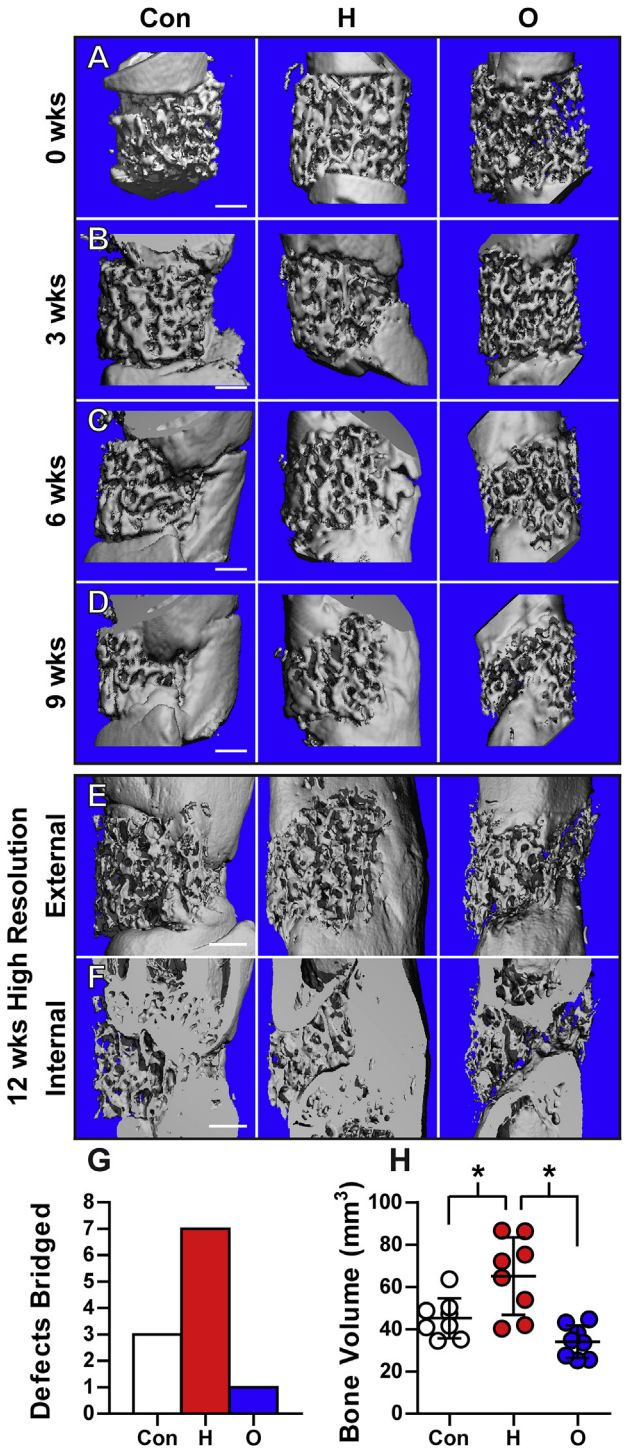

Fig. 3. Bridging of critically sized femoral defects. **A** Representative three-dimensional μCT reconstructions of the rat femur at day 1, 3 weeks, 6 weeks, 9 weeks and 12 weeks post-implantation for all three groups: acellular scaffolds *(Con)*, hypertrophic chondrocyte *(H)* and osteoblast *(O)* grafts. Internal and external regions are shown for 12 weeks (**E-F**). H grafts demonstrated the most complete femur regeneration demonstrated by defect bridging (**G**) and total bone volume deposited at 12 weeks (**H**). Scale bar: 1 cm. Value ± SD. Significant differences: $^{*}p < 0.05$ (n = 8).

grafts, but very little remodeling of the scaffold. By 9 weeks, most H and some Con grafts have bridged the defect, in contrast to the O grafts that displayed large fissures (Fig. 3D). The H grafts underwent substantial remodeling, with deposition of the new matrix, and formation of bone bridges along the medial side of the graft. The O grafts showed integration with only minimal remodeling, and appeared fragmented. The Con grafts had substantial deposition along the medial exterior; however, only minimal bone had been formed within the acellular scaffold and defect space.

High-resolution μCT scans (10 μm resolution) taken at the 12-week endpoint of implantation (Fig. 3E and F) revealed substantial differences in healing between the three groups. The exterior of the H grafts underwent extensive remodeling, integrated seamlessly into the femur, and contained large regions resembling native bone. Interior reconstruction demonstrated a thick, cortical-like bridge that formed along the medial segment of the graft. The O grafts lacked remodeling of the exterior zone and displayed severe lack of new bone matrix, fissures, and only minimal integration. In most cases, these grafts failed to facilitate defect bridging and regeneration. Con grafts facilitated some defect bridging and induced partial integration with the host bone. As determined through the post-harvest μCT, 7/8 of H grafts, 1/8 of O grafts, and 3/8 of Con grafts bridged the defect (Fig. 3G). H grafts were associated with enhanced total mineral presence in the defect space, as shown by the greater total bone volume in the defect space (Fig. 3H).

3.3. Bone formation and regeneration

Hard bone histology was used to visualize the components of the regenerated defects. Newly deposited bone (NB, fuchsia), the implanted scaffold (DCB, light pink), and fibrous tissue (FT, pale yellow) could be identified (Fig. 4A). Magnified views revealed bone marrow (BM, blue) and calcified cartilage (CC, dark purple) regions (Fig. 4B). The presence of cartilage within the defect space indicates the use of endochondral ossification in the regeneration of the defect. Movat's pentachrome, in which cartilage is stained green, was utilized and demonstrated cartilage presence in all grafts, regardless of cellular differentiation (Fig. 4C). The enlarged, hypertrophic chondrocytes surrounded in cartilage matrix transitioning to the newly formed bone (yellow) indicated that endochondral ossification was involved in new bone formation in all grafts. Endochondral ossification was observed at the edges of the native femur within the Con and O grafts, and throughout the implant in H grafts.

New bone deposition histologically matched the mineral depositions visualized by μCT. H grafts displayed strong deposition of new bone. In the O grafts, new bone was localized at the integration sites and in part in the defect space. In Con grafts, new bone deposition was localized at the integration sites and the medial side of the graft. The magnified views demonstrated that the new bone was formed around the scaffold, rather than replacing it. Semi-quantitation of the samples revealed similar amounts of the original scaffold present in all three groups (Fig. 4D). The extent of bone formation varied, with the H grafts containing significantly more new bone and bone marrow (Fig. 4D), and significantly less fibrous tissue (Fig. 4D) than either control, indicating advanced bone regeneration.

M2 macrophages are integral to long bone regeneration, providing a pro-repair environment that aids in enhanced defect regeneration [40]. Immunohistochemistry staining of CD163 demonstrated the significantly increased presence of M2 macrophages within the H graft defect space (Fig. 5).

Osteoclasts, a critical factor in bone regeneration, were identified by their multinucleation and Howship's lacunae, and were counted within the defect space of each graft. As seen in Fig. 6A, there was a tendency for osteoclasts to resorb DCB scaffolds located within the fibrous tissue of failed regeneration sites, with the H grafts containing significantly less osteoclasts overall (Fig. 6B). The ratio of osteoclasts digesting DCB matrix to the overall DCB area was calculated, and the H grafts once again had significantly less

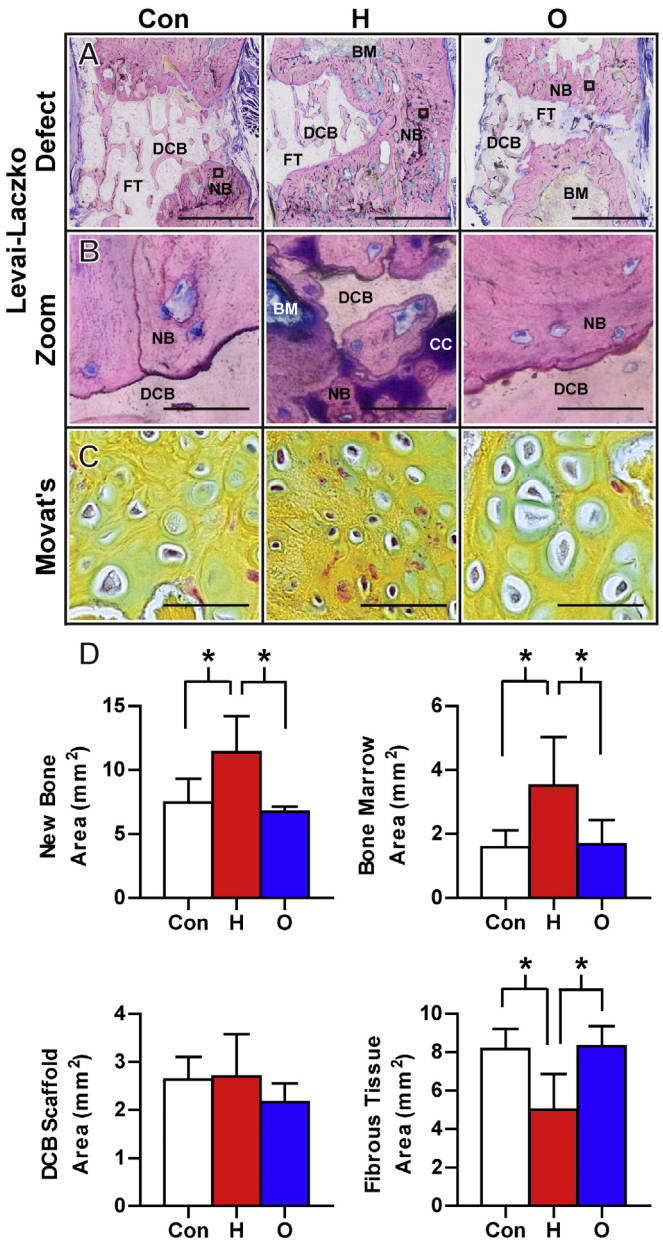

Fig. 4. Defect regeneration. Bone formation is shown at 12 weeks post-implantation. **A** Hard bone histology using the Levai-Laczko stain demonstrated the overall morphology of the defect region and differences between the scaffold material (DCB), newly deposited bone (NB), fibrous tissue (FT), and bone marrow (BM). In the Con graft, new bone deposition was largely constrained to the medial side at the integration sites. New bone deposition was widespread in the H graft, with some implanted scaffold material still present in the defect zone. In the O graft, new bone was located at the leading edge of the native skeleton, with minimal amounts of implanted scaffold scattered throughout the defect. **B** Magnified views allowed detection of calcified cartilage (CC), an important intermediate in endochondral ossification that was seen extensively in the H grafts, which also contained numerous bone marrow regions. **C** At the location of new bone formation, a cartilage anlage characteristic of endochondral ossification was present in all three groups (green staining in Movat's pentachrome sections). The images demonstrate turnover of cartilage (green) into newly deposited bone template (yellow). **D** There was a significantly higher presence of new bone and bone marrow within the H grafts. There was no significant difference in the amount of original DCB scaffold still remaining in the graft space, but there was significantly less fibrous tissue within the H grafts. Scale Bars: 2 mm (4A), 100 μm (4B), 50 μm (4C). Value ± SD. Significant differences between the groups * $p < 0.05$ ($n = 4$). (For interpretation of the references to colour in this figure legend, the reader is referred to the web version of this article.)

osteoclasts per area (Fig. 6C). Comparing the number of osteoclasts digesting DCB to new bone, the ratio for H grafts was significantly lower than in the other groups (Fig. 6D), indicating that the osteoclasts in H grafts were digesting newly deposited bone. The lower proportion of osteoclasts in H grafts, despite similar overall amounts of DCB, suggests a difference in repair environments amongst the graft types.

4. Discussion

Tissue engineering of autologous bone grafts has potential to provide effective repair of fracture non-unions, using methods customized to the patient and defect being treated [41]. Current efforts have proven to be insufficient for clinical translation due to various complications, including limited integration, incomplete regeneration, and poor mechanical properties of the grafts [7]. We hypothesized that these limitations could be overcome by using grafts based on differentiated hypertrophic chondrocytes engineered to withstand the challenging environment. We demonstrated the regenerative superiority of the hypertrophic chondrocyte grafts by (*i*) integration with adjacent native bone, (*ii*) more extensive bone deposition, (*iii*) more effective bridging of defects, and (*iv*) regenerative milieu established within the defect space.

Hypertrophic chondrocytes were differentiated from ASCs by modification of a previous protocol [18]. Rather than stopping after chondrocyte differentiation and cartilage anlage deposition, similar to previous studies [14,15,20], hypertrophic chondrocytes were matured, to markedly enhance mineral deposition and bone formation [18]. By maturing hypertrophic chondrocytes, chondrogenic and hypertrophic gene expression increased and substantial hypertrophic cartilage-like matrix was deposited within the scaffold pores (Fig. 1B). These results agreed with recent reports on hypertrophic chondrocytes [26,42].

Hypertrophic chondrocytes expressed bone-related genes [11,37,39] and when compared to the osteoblast-based grafts (Fig. 2), the differentiated hypertrophic chondrocytes showed elevated expression of these genes, consistent with expression values previously reported [43]. The differences in gene expression, though not correlated, are matched by differences in protein deposition, as the differentiated hypertrophic chondrocytes grafts had increased presence of BSP and OPN and deposited it in different locations within the graft (Fig. 2). The difference in behavior between the two cell types agrees with the putative roles of each cell type within the body. Hypertrophic chondrocytes are responsible for orchestrating large quantities of bone template deposition in a non-mineralized space [44], and the hypertrophic chondrocyte grafts showed similar behavior with deposition of the bone nucleating proteins of the bone template within the formed cartilage matrix located in the scaffold pore spaces (Fig. 2). Osteoblasts play a large role in modulating the existing bone [44], and the osteoblast grafts displayed similar behavior with osteoid deposition along the existing decellularized bone scaffold and only minimal matrix deposition within the scaffold pores (Fig. 2). The differences in expression and deposition experienced in this study might therefore be due to the natural scale of deposition each cell type is responsible for.

The orthotopic, critical-sized defect in the rat femur required considerable bone regeneration, and all three experimental groups demonstrated new bone formation through endochondral ossification. Similar to an earlier study in the rat calvaria [19] and the cell behavior pre-implantation, hypertrophic chondrocytes deposited significantly more bone than the osteoblasts in the long-bone fracture model (Fig. 3). Whereas hypertrophic chondrocyte-based grafts resulted in bridging 7/8 femoral defects, the osteoblast-

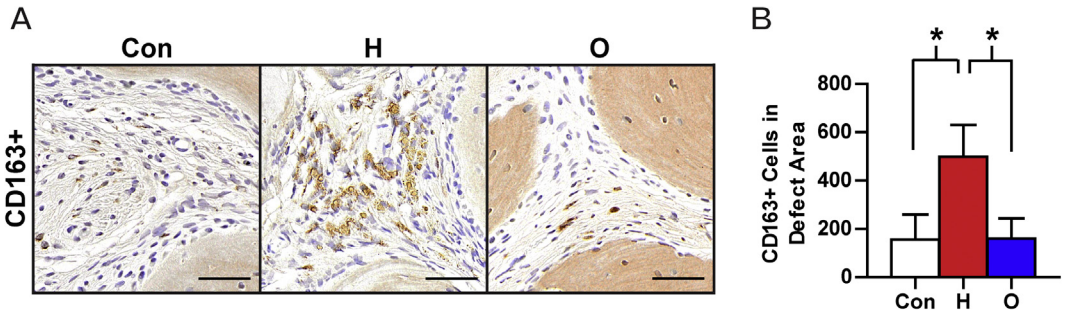

Fig. 5. M2 macrophages within the defect. A Histological sections of the defect were stained for M2 macrophages using a CD163 + antibody. **B** H grafts demonstrated significantly increased presence of M2 macrophages compared to the Con and O grafts (by CD163 + stain). Scale Bars: 50 μm. Value ± SD. Significant differences between the groups * $p < 0.05$ ($n = 3$).

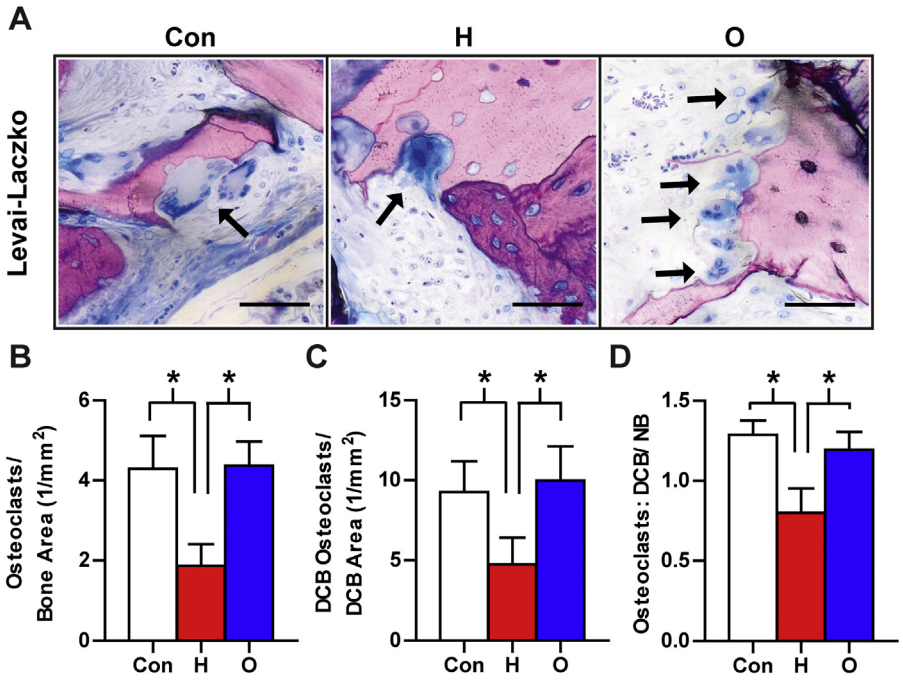

Fig. 6. Osteoclast presence and behavior within the defect. A Osteoclasts (black arrows) were determined by multinucleation and the formation of Howship's lacunae from the Levai-Laczko staining. Osteoclasts were located throughout all groups, on both the decellularized bone scaffold (light pink) and on newly deposited bone (fuchsia). **B** H grafts contained significantly less osteoclasts overall. **C** H grafts contained significantly lower amounts of osteoclasts resorbing the original DCB scaffold. **D** The ratio of osteoclasts found resorbing DCB scaffold to the osteoclasts found resorbing newly deposited bone was calculated and H grafts had a significantly lower ratio of DCB osteoclasts to new bone osteoclasts than the other two grafts. Scale Bars: 50 μm. Value ± SD. Significant differences between the groups * $p < 0.05$ ($n = 4$). (For interpretation of the references to colour in this figure legend, the reader is referred to the web version of this article.)

based grafts caused bridging of only 1/8 femoral defects (Fig. 3).

Clearly, large long bone defects present a complex signaling environment with the biological, structural and mechanical cues instigating repair through endochondral ossification [8,45]. The superior regeneration caused by the hypertrophic chondrocyte grafts is likely due to the progression of natural endochondral ossification, as was shown for femoral repair using pellets of chondrocytes implanted into the defect [15,16]. Lower amounts of GAG-rich matrix in the H grafts, coupled with the smaller lacunae of the cells, are consistent with the progression of endochondral regeneration (Fig. 4C), and resemble the resorption behavior detailed in the subcutaneous implantation of differentiated hypertrophic chondrocytes [43]. Late stage hypertrophic chondrocytes also regulate local osteoblast activity [46], and differentiated hypertrophic chondrocytes have been shown to influence cortical and trabecular-like bone formation [43]. Where decellularized hypertrophic cartilage matrix has demonstrated potential for bone formation [47], it has been shown that the release of cytokines (partially contained in the matrix) by the hypertrophic chondrocytes are essential for this bone formation and remodeling [19,48,49], thereby suggesting that increased, remodeled bone in the H grafts was orchestrated by the implanted hypertrophic chondrocytes. Recent publications have shown that during the end stages of endochondral ossification, hypertrophic chondrocytes can transdifferentiate into osteoblasts and osteocytes, cells that are smaller than hypertrophic chondrocytes [50–52] that can produce, remodel and maintain new bone matrix [51,52]. These publications suggested that the hypertrophic chondrocytes, besides orchestrating host cell behavior, could also have played a direct role in increasing bone deposition.

Macrophages are essential for endochondral ossification [53]. When M2 macrophages were induced in the fracture defect at later stages of endochondral ossification, bone formation was enhanced [54]. The H grafts had a significantly higher presence of M2

macrophages (Fig. 5), indicating the benefits of hypertrophic chondrocyte grafts in influencing a bone-forming environment. One potential reason for the higher count of M2 macrophages could be the extensive osteopontin deposition in the H grafts (Fig. 2), as osteopontin has been shown to influence macrophage behavior and M2 polarization [55]. Reinforcing an anabolic environment, the H grafts contained significantly less osteoclasts within the graft defect and induced less overall resorption (Fig. 6), in agreement with recent studies [19]. A significant portion of of the osteoclasts present within the defect were located within the deposited matrix, rather than in the original DCB scaffold (Fig. 6). The specific localization of osteoclasts and the enhanced remodeling, indicated by the seams within the H grafts, indicates the influence of the differentiated hypertrophic chondrocytes.

In addition to the regenerative environment, hypertrophic chondrocytes are integral to many other aspects of mature bone formation. Endochondral ossification is required for hematopoietic stem-cell niche formation, and studies have shown that suppressing hypertrophic progression inhibits niche formation [56]. Differentiated hypertrophic chondrocytes from MSCs facilitated bone marrow niche formation upon subcutaneous implantation [43], and it is the reversion of chondrocyte differentiation that supports the presence of stem cells within the niche [57]. When implanted orthotopically, hypertrophic chondrocyte grafts contained significantly more bone marrow compared to the other two groups (Fig. 4D).

Decellularized bone is an ideal biomaterial for bone regeneration, as it already contains the appropriate cell microenvironment, growth factors, and mechanical properties of bone [58]. Decellularized bone has shown ability to stimulate bone formation when implanted in calvarial defects, and to be osteogenic to the surrounding host cells [59]. This ability was readily apparent in this study in μCT reconstructions (Fig. 3), as new bone formation occurred surrounding the scaffold, areas rich in stem and progenitor cells. The deposition was exaggerated by the lower resolution *in vivo* μCT imaging (Fig. 3A–D), as the high resolution scans at 12 weeks demonstrated porous bone and quantifiably, significantly less total mineral than the H grafts.

Despite these known abilities of decellularized bone, it was surprising that the acellular control scaffolds performed better than the osteoblast-based scaffolds. We believe the poor performance was due to the characteristics of the defect, as previous osteoblast-based tissue engineered bone has shown successful results [41]. This cited study demonstrated methodical bone regeneration by differentiated osteoblasts, with step-wise coordination of bone resorption and deposition at the graft-skeleton interface [41]. Within the defect, new bone deposition could be seen at the interfaces, and the new bone deposition lines could be determined in the internal section at 12 weeks (Fig. 3F). Interestingly, the O grafts didn't demonstrate heavy external, medial depositions like the H and Con grafts, potentially reinforcing the importance of graft-skeleton interface and the coordination of the osteoblasts. The mechanical loading exhibited on the defect appeared to overcome the mechanical stability of O grafts, as fissures formed in 7/8 of these grafts.

While significant bone was deposited in the H grafts, regeneration of the critical-sized defect remained incomplete. The bridging of only one side of the H grafts, and a clear bias towards one side in all grafts, is a typical phenomenon in long bone fracture repair that occurs in part to the mechanical stimulation gradient produced by the fixation [60]. The segment of the graft nearest to the internal fixator is stabilized and experiences only minimal forces, whereas the segments that are further away experience mechanical stimulation that is known to enhance bone regeneration [60]. As seen in μCT reconstructions (Fig. 2), the lateral side of the H grafts, adjacent to the internal fixator, formed the least amount of new bone while the medial side underwent extensive bone regeneration. The high degree of regeneration in the medial segment suggests that hypertrophic chondrocytes might be directly affected by mechanical stimulation. The use of fixators allowing uniform mechanical environment, such as those used for cortical locking [61], would allow more complete defect regeneration.

One significant limitation of this study was the sole harvest time point at 12 weeks, leaving the exact contributions of the implanted and host cells to bone regeneration inconclusive. Future studies should elucidate the exact mechanisms initiated in the long bone defect by hypertrophic chondrocytes and the distinct roles of the implanted and host cells and determine if they match the pre-existing work in other bone forming models [17,43,52]. Additional studies will also be needed to examine interactions between the implanted differentiated cells and the inflammatory milieu. While allogeneic cells have obvious commercial potential, better performance of autografts in long bone grafting [2] suggests that autologous cells present the preferred clinical option.

In summary, we found that hypertrophic chondrocytes enhance regeneration in critical-size, orthotopic long bone defects. The use of critical-size femoral defects in a rat model demonstrates the feasibility and promise of the differentiated hypertrophic chondrocyte grafts [62]. Because rats do not display haversian-type remodeling in the cortex [63], translation to the human bone model needs to be undertaken to extend the predictive power of the results of these studies. Large animal studies are certainly needed before translation to human trials; however, the positive repair environment with rapid bone deposition and integration into the native skeleton that was superior to the performance of both acellular scaffolds and the traditional, osteoblast-based tissue engineered grafts, warrants further study for long bone fracture repair.

Acknowledgment

We gratefully acknowledge the NIH funding support of this work (grants EB002520, DE016525, and AR061988). We thank Dr. Andrea Lindenmair, Dr. Eleni Priglinger, and Dr. Susanne Wolbank for the harvest, isolation, and characterization of adipose derived stem cells. We also thank Gabriele Leinfellner for *in vivo* computed tomography imaging of the rats, and Dominika Lidinsky and Dr. Sylvia Nuernberger for their help in preparation and staining of paraffin-embedded histological sections. We also thank Prof. Mag. Dr. Dominik Ruenzler for the use of his laboratory space and facilities at the University of Applied Sciences Technikum Wien, Vienna.

Appendix A. Supplementary data

Supplementary data related to this article can be found at http://dx.doi.org/10.1016/j.biomaterials.2017.05.045.

References

[1] J.A. Bishop, A.A. Palanca, M.J. Bellino, D.W. Lowenberg, Assessment of compromised fracture healing, J. Am. Acad. Orthop. Surg. 20 (2012) 273–282.
[2] M.A. Flierl, W.R. Smith, C. Mauffrey, K. Irgit, A.E. Williams, E. Ross, et al., Outcomes and complication rates of different bone grafting modalities in long bone fracture nonunions: a retrospective cohort study in 182 patients, J. Orthop. Surg. Res. 8 (2013) 33.
[3] Albee FH. Evolution of bone graft surgery. Am. J. Surg. 63: 421–436.
[4] R. Langer, J.P. Vacanti, Tissue engineering, Science 260 (1993) 920–926.
[5] C.T. Laurencin, A.M.A. Ambrosio, M.D. Borden, J.A. Cooper, Tissue engineering: orthopedic applications, Annu. Rev. Biomed. Eng. 1 (1999) 19–46.
[6] A.J. Salgado, O.P. Coutinho, R.L. Reis, Bone tissue engineering: state of the art and future trends, Macromol. Biosci. 4 (2004) 743–765.
[7] A.R. Amini, C.T. Laurencin, S.P. Nukavarapu, Bone tissue engineering: recent

advances and challenges, Crit. Rev. Biomed. Eng. 40 (2012) 363–408.
[8] P. Bianco, F.D. Cancedda, M. Riminucci, R. Cancedda, Bone formation via cartilage models: the “borderline” chondrocyte, Matrix Biol. 17 (1998) 185–192.
[9] L.C. Gerstenfeld, D.M. Cullinane, G.L. Barnes, D.T. Graves, T.A. Einhorn, Fracture healing as a post-natal developmental process: molecular, spatial, and temporal aspects of its regulation, J. Cell. Biochem. 88 (2003) 873–884.
[10] T.A. Einhorn, The cell and molecular biology of fracture healing, Clin. Orthop. Rel Res. (1998) S7–S21.
[11] M.B. Goldring, K. Tsuchimochi, K. Ijiri, The control of chondrogenesis, J. Cell. Biochem. 97 (2006) 33–44.
[12] S.C. Dennis, C.J. Berkland, L.F. Bonewald, M.S. Detamore, Endochondral ossification for enhancing bone regeneration: converging native extracellular matrix biomaterials and developmental engineering in vivo, Tissue Eng. B Rev. 21 (2015) 247–266.
[13] E. Farrell, S.K. Both, K.I. Odorfer, W. Koevoet, N. Kops, F.J. O'Brien, et al., In-vivo generation of bone via endochondral ossification by in-vitro chondrogenic priming of adult human and rat mesenchymal stem cells, BMC Musculoskel. Disord. 12 (2011) 31.
[14] E. Farrell, O.P. van der Jagt, W. Koevoet, N. Kops, C.J. van Manen, C.A. Hellingman, et al., Chondrogenic priming of human bone marrow stromal cells: a better route to bone repair? Tissue Eng. C Meth. 15 (2009) 285–295.
[15] J. van der Stok, M.K. Koolen, H. Jahr, N. Kops, J.H. Waarsing, H. Weinans, et al., Chondrogenically differentiated mesenchymal stromal cell pellets stimulate endochondral bone regeneration in critical-sized bone defects, Eur. Cell. Mater. 27 (2014) 137–148 discussion 48.
[16] N. Harada, Y. Watanabe, K. Sato, S. Abe, K. Yamanaka, Y. Sakai, et al., Bone regeneration in a massive rat femur defect through endochondral ossification achieved with chondrogenically differentiated MSCs in a degradable scaffold, Biomaterials 35 (2014) 7800–7810.
[17] K. Bardsley, A. Kwarciak, C. Freeman, I. Brook, P. Hatton, A. Crawford, Repair of bone defects in vivo using tissue engineered hypertrophic cartilage grafts produced from nasal chondrocytes, Biomaterials 112 (2017) 313–323.
[18] C. Scotti, B. Tonnarelli, A. Papadimitropoulos, A. Scherberich, S. Schaeren, A. Schauerte, et al., Recapitulation of endochondral bone formation using human adult mesenchymal stem cells as a paradigm for developmental engineering, Proc. Natl. Acad. Sci. U. S. A. 107 (2010) 7251–7256.
[19] E.M. Thompson, A. Matsiko, D.J. Kelly, J.P. Gleeson, F.J. O'Brien, An endochondral ossification-based approach to bone repair: chondrogenically primed mesenchymal stem cell-laden scaffolds support greater repair of critical-sized cranial defects than osteogenically stimulated constructs in vivo, Tissue Eng. A 22 (2016) 556–567.
[20] K. Pelttari, A. Winter, E. Steck, K. Goetzke, T. Hennig, B.G. Ochs, et al., Premature induction of hypertrophy during in vitro chondrogenesis of human mesenchymal stem cells correlates with calcification and vascular invasion after ectopic transplantation in SCID mice, Arthritis Rheum. 54 (2006) 3254–3266.
[21] E.J. Sheehy, T. Mesallati, L. Kelly, T. Vinardell, C.T. Buckley, D.J. Kelly, Tissue engineering whole bones through endochondral ossification: regenerating the distal phalanx, Biores Open Access 4 (2015) 229–241.
[22] D.J. Hak, D. Fitzpatrick, J.A. Bishop, J.L. Marsh, S. Tilp, R. Schnettler, et al., Delayed union and nonunions: epidemiology, clinical issues, and financial aspects, Injury 45 (Suppl. 2) (2014) S3–S7.
[23] G. Pachon-Pena, G. Yu, A. Tucker, X. Wu, J. Vendrell, B.A. Bunnell, et al., Stromal stem cells from adipose tissue and bone marrow of age-matched female donors display distinct immunophenotypic profiles, J. Cell. Physiol. 226 (2011) 843–851.
[24] J. Gimble, F. Guilak, Adipose-derived adult stem cells: isolation, characterization, and differentiation potential, Cytotherapy 5 (2003) 362–369.
[25] R. Osinga, N. Di Maggio, A. Todorov, N. Allafi, A. Barbero, F. Laurent, et al., Generation of a bone organ by human adipose-derived stromal cells through endochondral ossification, Stem cells Transl. Med. 5 (2016) 1090–1097.
[26] J.M. Jukes, S.K. Both, A. Leusink, L.M.T. Sterk, C.A. Van Blitterswijk, J. De Boer, Endochondral bone tissue engineering using embryonic stem cells, Proc. Natl. Acad. Sci. U. S. A. 105 (2008) 6840–6845.
[27] M.B. Mueller, R.S. Tuan, Functional characterization of hypertrophy in chondrogenesis of human mesenchymal stem cells, Arthritis Rheum. 58 (2008) 1377–1388.
[28] W.L. Grayson, S. Bhumiratana, C. Cannizzaro, P.H.G. Chao, D.P. Lennon, A.I. Caplan, et al., Effects of initial seeding density and fluid perfusion rate on formation of tissue-engineered bone, Tissue Eng. A 14 (2008) 1809–1820.
[29] W.L. Grayson, M. Froehlich, K. Yeager, S. Bhumiratana, M.E. Chan, C. Cannizzaro, et al., Engineering anatomically shaped human bone grafts, Proc. Natl. Acad. Sci. U. S. A. 107 (2010) 3299–3304.
[30] I. Marcos-Campos, D. Marolt, P. Petridis, S. Bhumiratana, D. Schmidt, G. Vunjak-Novakovic, Bone scaffold architecture modulates the development of mineralized bone matrix by human embryonic stem cells, Biomaterials 33 (2012) 8329–8342.
[31] P. Bourin, B.A. Bunnell, L. Casteilla, M. Dominici, A.J. Katz, K.L. March, et al., Stromal cells from the adipose tissue-derived stromal vascular fraction and culture expanded adipose tissue-derived stromal/stem cells: a joint statement of the international federation for adipose therapeutics and science (IFATS) and the international society for cellular therapy (ISCT), Cytotherapy 15 (2013) 641–648.
[32] M. Frohlich, W.L. Grayson, D. Marolt, J.M. Gimble, N. Kregar-Velikonja, G. Vunjak-Novakovic, Bone grafts engineered from human adipose-derived stem cells in perfusion bioreactor culture, Tissue Eng. A 16 (2010) 179–189.
[33] O.B. Betz, V.M. Betz, A. Abdulazim, R. Penzkofer, B. Schmitt, C. Schroder, et al., The repair of critical-sized bone defects using expedited, autologous BMP-2 gene-activated fat implants, Tissue Eng. A 16 (2010) 1093–1101.
[34] T. Aigner, K.R. Greskotter, J.C.T. Fairbank, K. von der Mark, J.P.G. Urban, Variation with age in the pattern of type X collagen expression in normal and scoliotic human intervertebral discs, Calcif. Tissue Int. 63 (1998) 263–268.
[35] K. Donath, Die Trenn-Dünnschliff-Technik zur Herstellung histologischer Präparate von nicht schneidbaren Geweben und Materialien, Der Präparator 34 (1988) 197–206.
[36] J.L.G. Levai, A simple differential staining method for semi-thin sections of ossifying cartilage and bone tissues embedded in epoxy resin, Microscopy 31 (1975) 1–4.
[37] H. Chen, F.Y. Ghori-Javed, H. Rashid, M.D. Adhami, R. Serra, S.E. Gutierrez, et al., Runx2 regulates endochondral ossification through control of chondrocyte proliferation and differentiation, J. Bone Miner. Res. Official J. Am. Soc. Bone Miner. Res. 29 (2014) 2653–2665.
[38] G. Karsenty, Role of Cbfa1 in osteoblast differentiation and function, Semin. Cell Dev. Biol. 11 (2000) 343–346.
[39] L.C. Gerstenfeld, F.D. Shapiro, Expression of bone-specific genes by hypertrophic chondrocytes: implication of the complex functions of the hypertrophic chondrocyte during endochondral bone development, J. Cell. Biochem. 62 (1996) 1–9.
[40] A.C. Wu, L.J. Raggatt, K.A. Alexander, A.R. Pettit, Unraveling macrophage contributions to bone repair, BoneKEy Rep. 2 (2013).
[41] S. Bhumiratana, J.C. Bernhard, D.M. Alfi, K. Yeager, R.E. Eton, J. Bova, et al., Tissue-engineered autologous grafts for facial bone reconstruction, Sci. Transl. Med. 8 (2016).
[42] E.J. Sheehy, T. Mesallati, L. Kelly, T. Vinardell, C.T. Buckley, D.J. Kelly, Tissue engineering whole bones through endochondral ossification: regenerating the distal phalanx, BioResearch Open Access 4 (2015) 229–241.
[43] C. Scotti, E. Piccinini, A. Papadimitropoulos, P. Bourgine, A. Todorov, M. Mumme, et al., Engineering a bone organ through endochondral ossification, J. Tissue Eng. Regen. Med. 6 (2012) 30.
[44] B.R. Olsen, A.M. Reginato, W.F. Wang, Bone development, Annu. Rev. Cell. Dev. Biol. 16 (2000) 191–220.
[45] A. Boccaccio, C. Pappalettere, Mechanobiology of Fracture Healing: Basic Principles and Applications in Orthodontics and Orthopaedics, INTECH Open Access Publisher, 2011.
[46] A. Houben, D. Kostanova-Poliakova, M. Weissenböck, J. Graf, S. Teufel, K. von der Mark, et al., β-catenin Activity in Late Hypertrophic Chondrocytes Locally Orchestrates Osteoblastogenesis and Osteoclastogenesis. Development, 2016.
[47] G.M. Cunniffe, T. Vinardell, J.M. Murphy, E.M. Thompson, A. Matsiko, F.J. O'Brien, et al., Porous decellularized tissue engineered hypertrophic cartilage as a scaffold for large bone defect healing, Acta Biomater. 23 (2015) 82–90.
[48] P.E. Bourgine, C. Scotti, S. Pigeot, L.A. Tchang, A. Todorov, I. Martin, Osteoinductivity of engineered cartilaginous templates devitalized by inducible apoptosis, Proc. Natl. Acad. Sci. U. S. A. 111 (2014) 17426–17431.
[49] H.P. Gerber, T.H. Vu, A.M. Ryan, J. Kowalski, Z. Werb, N. Ferrara, VEGF couples hypertrophic cartilage remodeling, ossification and angiogenesis during endochondral bone formation, Nat. Med. 5 (1999) 623–628.
[50] L. Yang, K.Y. Tsang, H.C. Tang, D. Chan, K.S.E. Cheah, Hypertrophic chondrocytes can become osteoblasts and osteocytes in endochondral bone formation, Proc. Natl. Acad. Sci. U. S. A. 111 (2014) 12097–12102.
[51] X. Zhou, K. von der Mark, S. Henry, W. Norton, H. Adams, B. de Crombrugghe, Chondrocytes transdifferentiate into osteoblasts in endochondral bone during development, postnatal growth and fracture healing in mice, PLoS Genet. 10 (2014) 20.
[52] C.S. Bahney, D.P. Hu, A.J. Taylor, F. Ferro, H.M. Britz, B. Hallgrimsson, et al., Stem cell- derived endochondral cartilage stimulates bone healing by tissue transformation, J. Bone Min. Res. 29 (2014) 1269–1282.
[53] L.J. Raggatt, M.E. Wullschleger, K.A. Alexander, A.C.K. Wu, S.M. Millard, S. Kaur, et al., Fracture healing via periosteal callus formation requires macrophages for both initiation and progression of early endochondral ossification, Am. J. Pathol. 184 (2014) 3192–3204.
[54] C. Schlundt, T. El Khassawna, A. Serra, A. Dienelt, S. Wendler, H. Schell, et al., Macrophages in bone fracture healing: their essential role in endochondral ossification, Bone (2015), http://dx.doi.org/10.1016/j.bone.2015.10.019 [Epub ahead of print].
[55] C.-N. Lin, C.-J. Wang, Y.-J. Chao, M.-D. Lai, Y.-S. Shan, The significance of the co-existence of osteopontin and tumor-associated macrophages in gastric cancer progression, BMC Canc. 15 (2015) 128.
[56] C.K.F. Chan, C.-C. Chen, C.A. Luppen, J.-B. Kim, A.T. DeBoer, K. Wei, et al., Endochondral ossification is required for haematopoietic stem-cell niche formation, Nature 457 (2009), 490–U9.
[57] M. Serafini, B. Sacchetti, A. Pievani, D. Redaelli, C. Remoli, A. Biondi, et al., Establishment of bone marrow and hematopoietic niches in vivo by reversion of chondrocyte differentiation of human bone marrow stromal cells, Stem Cell Res. 12 (2014) 659–672.
[58] L. Polo-Corrales, M. Latorre-Esteves, J.E. Ramirez-Vick, Scaffold design for bone regeneration, J. Nanosci. Nanotechnol. 14 (2014) 15–56.
[59] D.J. Lee, S. Diachina, Y.T. Lee, L. Zhao, R. Zou, N. Tang, et al., Decellularized bone matrix grafts for calvaria regeneration, J. Tissue Eng. 7 (2016),

2041731416680306.
[60] M. Bottlang, F. Feist, Biomechanics of far cortical locking, J. Orthop. Trauma 25 (2011) S21–S28.
[61] M. Bottlang, M. Lesser, J. Koerber, J. Doornink, B. von Rechenberg, P. Augat, et al., Far cortical locking can improve healing of fractures stabilized with locking plates, J. Bone Jt. Surg.-Am. Vol. 92A (2010) 1652–1660.
[62] V. Viateau, D. Logeart-Avramoglou, G. Guillemin, H. Petite, Animal models for bone tissue engineering purposes, in: P.M. Conn (Ed.), Sourcebook of Models for Biomedical Research, Humana Press, Totowa, NJ, 2008, pp. 725–736.
[63] Y. Li, S.-K. Chen, L. Li, L. Qin, X.-L. Wang, Y.-X. Lai, Bone defect animal models for testing efficacy of bone substitute biomaterials, J. Orthop. Transl. 3 (2015) 95–104.